MULTI-LOOK PROCESSING FOR COHERENT CHANGE DETECTION WITH SYNTHETIC APERTURE SONAR

Vincent Myers[a,d], Johannes Groen[b], Holger Schmaljohann[c], Isabelle Quidu[d], Benoit Zerr[d]

[a] Defence R&D Canada, 9 Grove St., Halifax, Nova Scotia, B2Y 3Z7, Canada.
[b]ATLAS ELEKTRONIK GmbH, Sebaldsbruecker Heerstr. 235, 28309 Bremen, Germany.
[c] Bw Technical Centre for Ships and Naval Weapons, Maritime Technology and Research (WTD 71), Berliner Str. 115, 24340 Eckernförde, Germany.
[d] Lab-STICC, UMR CNRS 6285, PRASYS Group, ENSTA-Bretagne, Brest, France.

vincent.myers@drdc-rddc.gc.ca
johannes.groen@atlas-elektronik.com
holgerschmaljohann@bundeswehr.org
isabelle.quidu@ensta-bretagne.fr
benoit.zerr@ensta-bretagne.fr

Abstract: *The detection of changes in sets of serial images acquired at different times is a common approach used in the context of underwater surveillance and monitoring. Coherent change detection with Synthetic Aperture Sonar (SAS) involves using both phase and amplitude of the data to detect very subtle scene changes that may not be detectable from the magnitude of the mean backscattered power. This paper briefly examines some of the parameters used during the co-registration process, which determine the shape of the warping surface used to resample the repeat-pass image onto the original image, using standard statistical metrics that can evaluate the quality of the image registration. Using the results of this analysis, a multi-look processing approach which produces a set of ℓ independent looks of the scene is proposed in order to enhance the underlying coherence of the scene and improve the detection performance over that of a single-look image. The technique is tested on a data set collected in the Mediterranean Sea over sand ripples using ATLAS Elektronik's Vision 1200 system, a 150 kHz SAS mounted on the SeaOtter Autonomous Underwater Vehicle. Results show that it is possible to detect sub-resolution coherent changes under these environmental conditions using the proposed approach, and a number of recommendations for processing repeat-pass SAS data are made.*
Keywords: *Synthetic Aperture Sonar, Coherent Change Detection, Co-registration*

1. INTRODUCTION

The detection of changes in sets of serial images acquired at different times is a technique that has been applied across many disciplines that require surveillance and monitoring of a scene [1], and automated methods for both real and synthetic aperture sonar (SAS) have been a topic of research for several years [2][3]. Techniques fall into two broad categories: a) Contact-based, where newly acquired detections are associated with historical ones based on their absolute position, or relative to other objects in the scene; and b) Image-based, where the image pixels are directly compared. The latter category can be further divided into incoherent change detection (ICD) methods, where only the magnitude of the mean backscattered energy is used [4] or coherent change detection (CCD) methods, where differences in the interferometric phase of the images are used to detect changes caused by sub-resolution scattering processes that may not be visible in the mean backscatter images [5]. The challenges in underwater CCD are the same as those found in the more mature field of space or aircraft-based Synthetic Aperture Radar (SAR) systems, in particular robust co-registration, temporal decorrelation, and complex environments. These are made more difficult due to the stability and velocity of the platforms relative to the speed of sound and the dynamic underwater environment at the scale of the wavelengths of high-frequency ($\geq$ 80 kHz) SAS sensors. Nevertheless, the few studies where CCD methods have been applied to SAS images have demonstrated an ability to detect changes in the environment for temporal baselines of over a week [6][7].

This paper presents results of SAS CCD processing techniques for co-registration and detection demonstrated on a data set collected using the Vision 1200 SAS, manufactured by ATLAS Elektronik, whose HF option operates at a centre frequency $f_c = 150$ kHz. The images were collected in May of 2014 during an Italian MINEX in the Mediterranean Sea off the Western Coast of Italy over a field of medium sand ripples where several targets were removed following a baseline survey with targets. The temporal separation between the surveys was roughly 22 hours. One of the SAS images containing targets is shown in Figure 1.

The first part of this paper examines the parameters of the method used for finding matching control points and estimating the warping function required for the co-registration process, which considers both incoherent and coherent approaches. Section 3 introduces the use of multi-look processing to improve the robustness of the coherence estimate. Section 4 will look at the results of ICD and CCD techniques on the Vision 1200 data. The main findings of this work are summarized in Section 5, followed by suggestions for future research avenues.

2. CO-REGISTRATION PARAMETERS

One of the primary challenges in SAS CCD methods is the co-registration of the original (I_o) and repeat-pass (I_{rp}) images accurately enough to permit the interferometric processing required to detect changes in the coherence of the scene. This requirement is typically considered to be to within a fraction of the acoustic wavelength ($\lambda/8 - \lambda/10$, where $\lambda = c/f$ and c is the speed of sound and f is the frequency) [5] and is a mitigatable cause of coherence loss. While many co-registration techniques have been proposed, most start by determining a set of matching control points using a function $v(I_o, I_{rp}) \rightarrow [\delta_x, \delta_y]$ which returns a set of offsets in range and azimuth. Then, a function $w(\delta_x, \delta_y, I_{rp}) \rightarrow I_{cr}$ produces the co-registered image I_{cr}, which is used to produce the final interferometric

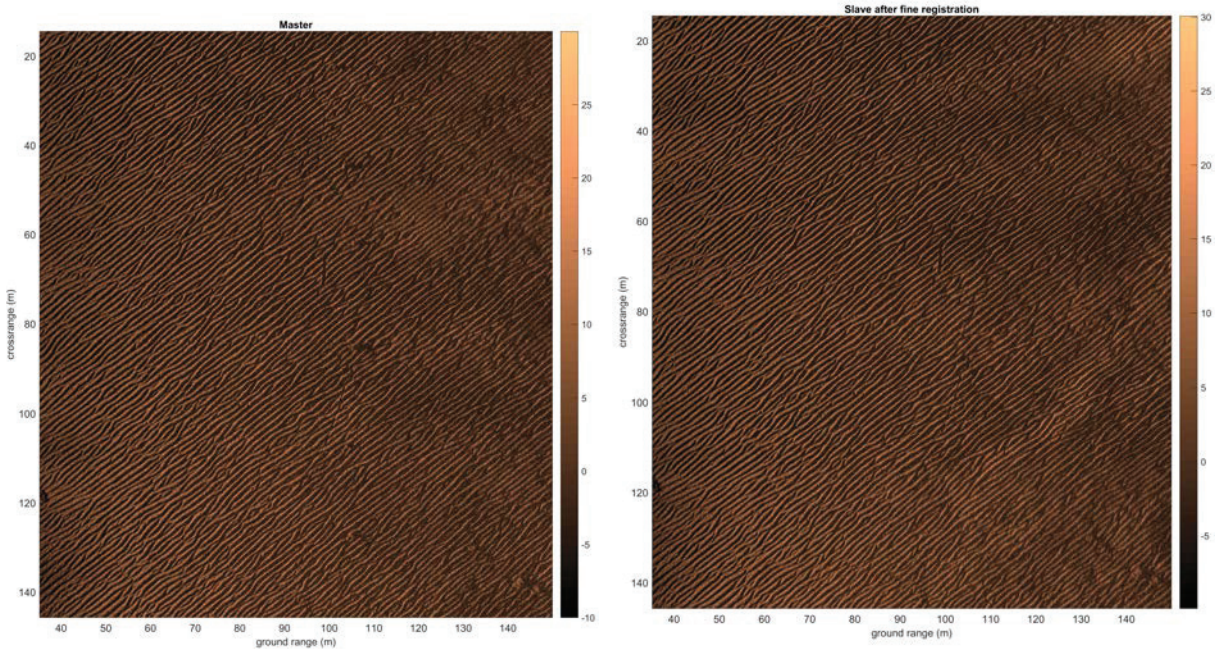

(a) *(b)*

Figure 1: (a) gives the original Vision 1200 SAS image showing an area of sand ripples and seven deployed targets. In (b) the repeat-pass image is shown, with the targets removed. The temporal baseline between the repeat-pass and original image is roughly one day (22 hours).

image $I_f = I_o I_{cr}^*$, where the * denotes the complex conjugate. The function w can make use of track registration or re-navigation of the data, however, a simple and direct method is to resample or warp I_{rp} onto I_o using a suitable interpolation function. Proposed approaches for v are the SIFT/SURF transforms [7], various forms of coherence [6] as well as others. The magnitude of the complex and amplitude-only correlation coefficient are considered here.

The magnitude of the sample coherence in an N-sized window of the complex original and repeat-pass images for a given shift in azimuth and range by $\boldsymbol{\delta} = [\delta_x, \delta_y]$ is:

$$|\gamma_{\boldsymbol{\delta}}| = \frac{1}{N} \sum \frac{(g_n - \mu_g)(h_{n,\boldsymbol{\delta}}^* - \mu_h)}{\sigma_g \sigma_{h_{\boldsymbol{\delta}}}}, \text{for } g_n \in I_o, h_n \in I_{rp}. \tag{1}$$

where $h_{n,\boldsymbol{\delta}}^*$ is the complex conjugate of the shifted sub-image h, and μ and σ are the sample mean and standard deviation inside the window. It is a two-dimensional version of Pearson's correlation coefficient, and when applied to the magnitude images $|I_o|$ and $|I_{rp}|$ it is a common control-point matching method used in many image processing applications, called the normalized cross-correlation, which will be denoted as $\rho_{\boldsymbol{\delta}}$. For each pixel in the image, a range of values for δ_x and δ_y are considered and the maximum value of $\boldsymbol{\delta}$ for both $\gamma_{\boldsymbol{\delta}}$ and $\rho_{\boldsymbol{\delta}}$ are retained for computing the warping function. There is a heavy computational burden associated with calculating control points for each pixel of large, high-resolution SAS images such as those generated by the Vision 1200. An efficient algorithm based on integral images [10] was implemented which significantly improved the performance of those computations for the varying values of N. An evaluation of both estimators of the pixel shifts was performed as a function of some quality metrics that are applied to the resulting interferometric image I_f. Two commonly used metrics

are contrast and sharpness [8][9] defined within a image of size M as:

$$Q_c = \frac{\sigma_{|I_f|}}{\mu_{|I_f|}}, \tag{2}$$

and

$$Q_s = 20 \log_{10} \left(\frac{1}{M} \sum |I_f|^2 \right). \tag{3}$$

For the images of sand ripples examined here, the coherence estimates result in somewhat higher sharpness and coherence values for the interferometric image. An examination of the computed shifts shows greater noise providing evidence that the shifts obtained using γ-based values for small values of N are more robust and provide better estimates of the true co-registration parameters, however as N gets larger, the performance deteriorates. The same is true for the cross-correlation estimate. Q_c is perhaps a better estimate of image quality in the case of an image with large areas of shadow and it has been noted that Q_s [9] in the form presented in Equation (3) does not account for shadow zones enough. It was expected that ρ would provide more robust co-registration parameters in areas of low coherence, however this was not the case. Based on this analysis, γ-estimates using a window size of 128×128 were selected.

3. MULTI-LOOK PROCESSING

Multi-look processing is commonly used in the SAR community to reduce speckle in single-look images [11] and phase noise of interferometric images; it has also been applied to SAS imagery for similar reasons [12]. The idea is to generate a number of ℓ lower-resolution "looks" at the scene by filtering the discrete Fourier transform $F(k_x, k_y)$ of the complex SAS image by k_x into a number of sub-bands, where k_x and k_y are the wavenumbers in the azimuth and range dimensions [13]. The relationship $k_x = 2k \sin\theta$ and $k_y = 2k \cos\theta$, with $k = 2\pi/\lambda$, is used to cover the total signal bandwidth B and SAS integration angle θ_{int}. The wavenumber spectrum of one of the images, and the area of support for four bands, is shown in Figure 2 with $\theta_{\text{int}} \approx 12^\circ$ of processed beamwidth for the Vision 1200. The upper and lower limits for k_y are found using $k_c \pm B/2$, where $k_c = 2\pi/\lambda_c$ is the wavenumber at the center frequency of the sonar and B is the bandwidth. Many different strategies can be applied to exploit the multi-look images; the approach taken here is to generate a set of ℓ separate looks of the images $I_{o,\ell}$ and $I_{rp,\ell}$ and co-register them individually using the method outlined previously. Because the scene is composed of sand ripples, the directionality of the spatial coherence may be exploited, and the fusion of the coherence of the individual looks may offer improvements to the performance of CCD methods. For ICD, a standard approach is adopted of creating a despeckled image $I_{o,ml} = \sum |I_{o,\ell}|$ and $I_{rp,ml} = \sum |I_{rp,\ell}|$ using the incoherent sum of the multi-look images.

4. RESULTS

The results of the co-registration method and the corresponding coherence (computed in a 64×64 pixel moving window) on the full resolution images, shown in Figure 3(a), are first examined. Patches of the scene have maintained some temporal coherence during the intervening interval between surveys. It is also possible to distinguish areas of low coherence caused by the insertion of the targets (*c.f.* Figure 1) however they are mostly lost within larger areas of low coherence and are unlikely to be detected in an un-alerted scenario. There are also what appear to be horizontal strips of low coherence that may

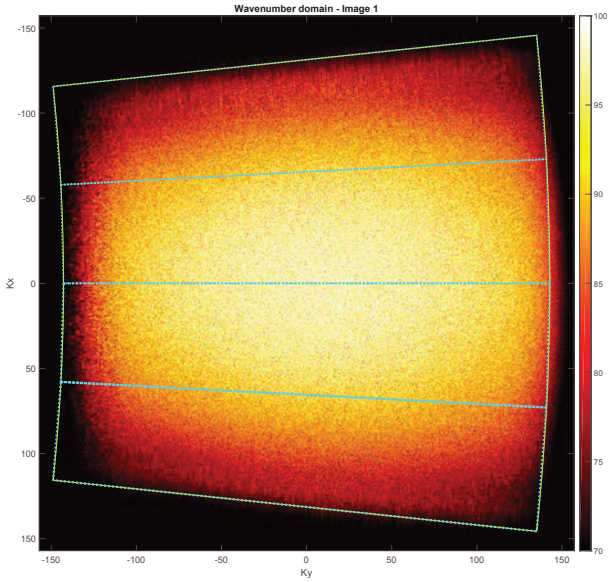

Figure 2: Wavenumber spectrum of the SAS image with the support area for each of the four looks.

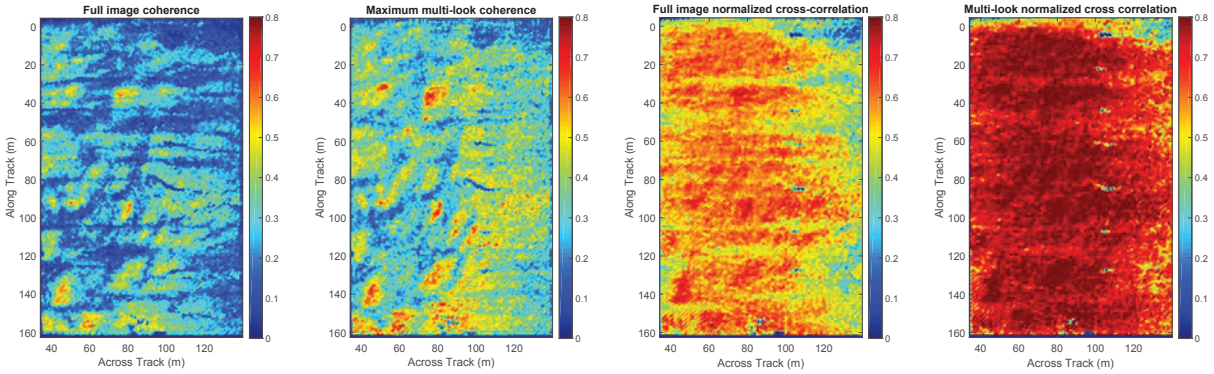

Figure 3: Results from the Vision 1200 SAS: (a) shows the coherence after co-registration of the full resolution image; (b) shows the maximum coherence for each pixel from each of the four looks; (c) shows the normalized cross-correlation between the full resolution co-registered original and repeat-pass images; and (d) the normalized cross-correlation for the multi-look image.

be artifacts caused by the SAS processing. In Figure 3(b) the results of the multi-look processing is shown for $\ell = 4$. For each pixel, the maximum of the coherence from each of the looks is chosen. By taking the maximum value, as well as the lower resolution of the multi-look images it is expected that the overall coherence should increase in areas with coherence in the full resolution images, and this is in fact observed. However, there are also areas which were not coherent in the full resolution images which have become coherent in at least one of the multi-look images, resulting in a better discrimination of the targets. Figure 3(c) shows the correlation coefficient for the co-registered multi-look images images $I_{o,ml}$ and $I_{rp,ml}$. By ignoring the phase information, the six deployed targets are more easily distinguished against the highly correlated and reduced-speckle background. For detecting changes on the order of the size of the targets deployed during this experiment, it is not strictly necessary to use the coherence between the images. In fact, ICD is likely to be more robust against a greater set of conditions than CCD under those circumstances. The appeal of CCD is the possibility of detecting scene changes

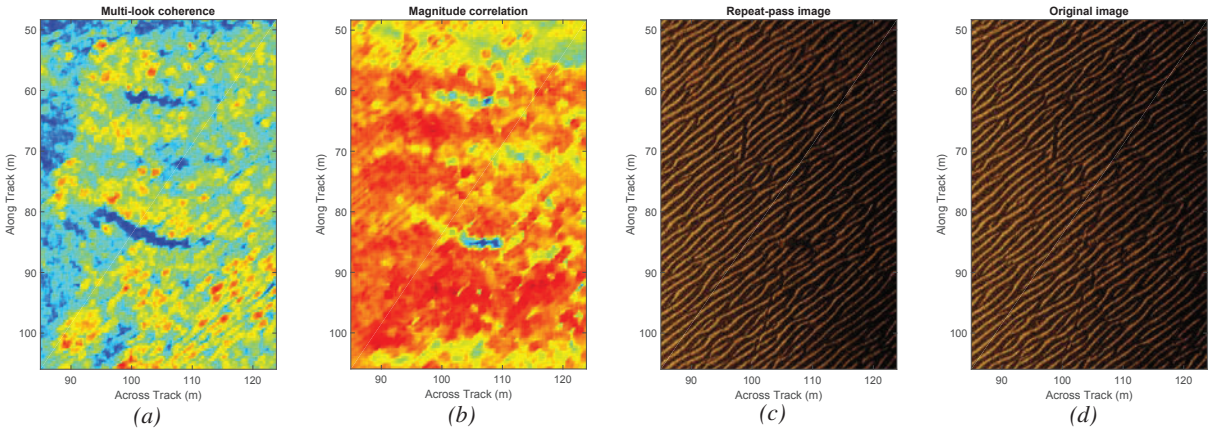

Figure 4: Panels (a) and (b) show the coherence and normalized cross-correlation, zoomed into targets 3 and 4. The corresponding original and repeat-pass images are shown in panels (c) and (d)

that are not detectable in the magnitude images, and some of these can be observed in the present data. Figure 4 shows the multi-look coherence of the complex images and the cross-correlation of the magnitude images from Figure 3, zoomed into the third and fourth targets from Figure 1. Also shown are the corresponding co-registered repeat-pass and original images. The drop in both coherence and correlation caused by the insertion of the targets into the scene are clearly visible. While the correlation focuses in on the mean backscatter changes caused by the physical presence of the targets, the coherence also indicates changes that do not appear to be visible in the magnitude images (shown on the right). While it is not possible to determine the exact cause of this change, as this was not part of the controlled variables of this experiment, two hypotheses are offered:

- The presence of sand ripples implies the presence of underwater currents. By placing these objects in the currents, a vortex may be created behind the objects which could have disturbed or otherwise reconfigured the speckle pattern behind the target. As the drop in coherence is roughly perpendicular to the ripple direction — the main direction of the currents needed to create these ripples — may be interpreted as evidence that supports this possibility.

- The targets may have been dragged during recovery, and the ripples were reformed with the underwater currents. These new ripples would have different speckle patterns, causing a drop in coherence.

In both cases, the drop in coherence is attributed to the effect of currents on the seabed at sub-resolution scales, which are then detectable through CCD means.

5. RECOMMENDATIONS AND FUTURE WORK

The principle findings of this work support the following recommendations:

- During co-registration, the use of coherence based-estimates for azimuth and range offsets generally resulted in more accurately co-registered image pairs. The window size used to estimate the co-registration parameters corresponded to roughly a 2.5×2.5 m patch of seafloor for this particular dataset with sand ripples. Using patches larger than this was not as effective.

- The multi-look processing method described here increased the overall coherence and resulted in simpler CCD. An examination of which look was chosen for which pixel (not shown in this paper) showed contiguous zones arranged horizontally, suggesting that the gain is not due to the directionality of the seabed but likely related to platform motion compensation.

- Large-scale objects are detected more easily using ICD on the magnitude images. Speckle reduction through multi-look processing increases the correlation between the images.

- Even in a dynamic underwater environment such as this one and using a relatively high-frequency sensor, it was possible to employ CCD methods to reveal scene changes that were not visible on the magnitude images.

This experiment has also provided valuable insight into the limitations and possibilities of underwater CCD. Suggestions for future research avenues are:

- Modeling of the underwater environment to understand the scope of changes that can be detected in practice using SAS CCD.

- A more thorough study of the effect of window size on the resulting co-registration quality is recommended as well as a comparision with other commonly used control point finding methods such as SIFT.

- More accurate models of the joint statistics of co-registered SAS images need to be developed in order to design optimal tests to carry out automated CCD in a robust fashion.

Finally, better control of the experimental conditions, while difficult, should be aspired to during future data collection, such that any observed changes in coherence can be better understood.

Acknowledgements
WTD 71 thanks CMRE for the opportunity to operate the AUV SeaOtter during the seatrial ITMINEX'14 from R/V Alliance.

REFERENCES

[1] **Radke, R.J., Andra, S., Al-Kofahi, O. and Roysam, B.,** "Image change detection algorithms: a systematic survey," *IEEE Transactions on Image Processing*, vol. 14(3), pp. 294-307, March 2005.

[2] **Sternlicht, D.D., Harbaugh, J.K. and Nelson, M.A.,** "Experiments in coherent change detection for synthetic aperture sonar," in *OCEANS 2009*, Biloxi, MI, 2009.

[3] **G-Michael, T. and Tucker, J.,** "Canonical correlation analysis for coherence change detection in synthetic aperture sonar imagery," in *Proceedings of the Institute of Acoustics*, vol. 32(4), pp. 117-122, 2010.

[4] **Midtgaard, Ø., Hansen, R.E., Sæbø, T., Myers, V., Dubberley, J.R., and Quidu, I.,** "Change detection using synthetic aperture sonar: Preliminary results from the Larvik trial," in *OCEANS 2011*, Kona, Hawaii, 2011.

[5] **Preiss, M. and Stacy, N.J.S.,** "Coherent change detection: theoretical description and experimental results," Tech. Rep. Defence Science and Technology Organisation (DSTO), 2006.

[6] **Myers, V., Quidu, I., Sæbø, T., and Hansen, R.E.,** "Results and analysis of coherent change detection experiments using repeat-pass synthetic aperture sonar," in *Underwater Acoustic Measurements (UAM) conference* , 2013.

[7] **G-Michael, T., Marchand, B., Tucker, J.D., Marston, T.M., Sternlicht, D.D., and Azimi-Sadjadi, M.R.,** "Image-based automated change detection for synthetic aperture sonar by multistage coregistration and canonical correlation analysis," *IEEE Journal of Oceanic Engineering*, vol. 41(3), pp. 592-612, 2016.

[8] **Marston, T., and Plotnick, D.,** "Semiparametric statistical stripmap synthetic aperture autofocusing", *IEEE Transactions on Geoscience and Remote Sensing*, 53(4), pp. 2086-2095, 2015.

[9] **Fienup, J. R., and Miller, J.J.,** "Aberration correction by maximizing generalized sharpness metrics", *Journal of the Optical Society of America*, 20(4), pp. 609-620, 2003.

[10] **Viola, P., and Jones, M.,**"Robust real-time object detection," *International Journal of Computer Vision*, vol. 57(2), pp. 137-154, 2004.

[11] **Jakowatz, C., Wahl, D., Eichel, P., Ghiglia, D., and Thompson, P.,** *Spotlight-Mode Synthetic Aperture Radar: A Signal Processing Approach*, Kluwer Academic Publishers, 1996.

[12] **Williams, D.P., and Hunter, A.J.,** "Multi-look processing of high-resolution SAS data for improved target detection performance," *IEEE International Conference on Image Processing (ICIP)*, Quebec City, Quebec, 2015.

[13] **Groen, J., Schmaljohann, H., Leier, S., Jans, W.,**"Synthetic aperture sonar fusion for images with dissimilar physical content due to differences in acoustic frequency," *Underwater Acoustics Conference and Exhibition (UACE)*, 2015.

[14] **Lyons, A.P., and Brown, D.C.,** "The impact of the temporal variability of seafloor roughness on synthetic aperture sonar repeat pass interferometry," *IEEE Journal of Oceanic Engineering*, vol. 38(1), pp. 91-97, 2013.